

Abstract

We have experimentally implemented two generalized quantum searching algorithms using NMR technique in a two qubits heteronuclear spin systems. In the first algorithm, the phase matching requirement is satisfied. In the second algorithm, the phase matching requirement is not satisfied. Both algorithms are run for 10 steps and the density matrices are constructed. It is found that in the first algorithm the marked state can be found, and in the 2nd experiment the algorithm failed to find the marked state. These are in good agreement with theoretical predication. Several issues arising in the experiment is addressed and discussed.

I. INTRODUCTION

Grover's quantum search algorithm is one of the most important development in quantum computation [1]. It achieves quadratic speedup in searching a marked state in an unordered list over classical searching algorithms. Classically, searching for a particular entry in an unordered list of N elements requires $O(N)$ attempts. Grover's quantum search algorithm can obtain the result with certainty in $O(\sqrt{N})$ attempts.

There are several generalizations of the Grover algorithm. First, in Grover's algorithm there is only one marked state. The marked state may not be a single one. If there are m marked state, the number of steps to find them is $O(\sqrt{N/m})$. Here it should be pointed out that the m marked states are not separated, rather they are clustered together. If you touches one of them, you then find them all. The task of finding m separated marked states requires running the algorithm m times and takes $m\sqrt{N}$ steps in total, more difficult than finding just one marked state.

Now let's explain briefly the phase matching requirement. During one search step in Grover's algorithm, there are two phase inversions. One is the phase inversion of the marked state and the other is the phase inversion of state $|0\rangle$. These inversions could be replaced by arbitrary phase rotations. However, they must be equal to one another, that is, the phases must match in order to succeed in quantum searching [3,4]. This generalization is of practical implication, because phase-matched small phase rotation leads to a smaller step in the searching process. This is useful when the search algorithm is approaching the marked state. Here we can use it to replace the ordinary Grover search algorithm so that the last step of search leads to exactly the marked state. In Grover's algorithm, the searching step is fixed and the state vector of the quantum computer is not exactly the marked state and the probability is not 1, a potential source of error when high accuracy is required.

Because of the simplicity of Grover's algorithm, it has been implemented in NMR quantum computers [5–7]. The experimental studies of quantum computing is important in demonstrating the power of quantum computing, investigating the effects of gate imperfections and decoherence, and demonstrating the effects of quantum error corrections. These knowledges are important for scaling-up a real and practical quantum computer. In this paper, we report the experimental studies in a 2 qubit heteronuclear system using NMR technique the effect of the phase matching requirement on quantum searching algorithm.

Two sets of experiment were performed. In the first set, a generalized phase matched quantum searching algorithm with $\theta = \phi = \pi/2$ is performed. In the second set, the phases do not match and we put $\theta = \pi/2$, $\phi = 3\pi/2$. In each set, ten steps were performed, and the density matrices were constructed. It is found that phase matching in quantum searching is crucial. The article is organized as follows. After this introduction, we will briefly review the algorithm in section 2. In section 3, the experimental procedures are described in details. In section 4, the results are presented and several issues arizing from this experimental work are discussed.

II. GENERALIZED QUANTUM SEARCHING ALGORITHM

Grover algorithm consists of essentially four steps in an iteration [2]: 1) a phase inversion of the prepared state $I_\gamma = I - 2|\gamma\rangle\langle\gamma|$, in our case $|\gamma\rangle = |0\rangle$; 2) a unitary transformation U . Usually U is taken the Walsh-Hadamard transformation $U=W$; 3) a phase inversion of the marked state $|\tau\rangle$, $I_\tau = I - 2|\tau\rangle\langle\tau|$; and 4) an inverse of the Walsh-Hadamard transformation $U^{-1} = W^{-1} = W$. The operator for one Grover iteration is $Q = -I_\gamma U^{-1} I_\tau U$.

We can see how Grover's quantum search algorithm works through the example with $N = 4$, which is the simplest interesting application of Grover's algorithm. It can be posed as follows: on the set $X = 00, 01, 10, 11$ (binary) a function $f(x) = 0$ except at some x_0 where $f(x_0) = 1$. Following Grover's procedure, first, prepare the initial state

$$|\psi_i\rangle = |00\rangle = \begin{pmatrix} 1 \\ 0 \\ 0 \\ 0 \end{pmatrix}. \quad (1)$$

Then we perform Walsh-Hadamard transform W on $|\psi_i\rangle$ to obtain

$$|\psi_0\rangle = W|\psi_i\rangle = \frac{1}{2} \begin{pmatrix} 1 & 1 & 1 & 1 \\ 1 & -1 & 1 & -1 \\ 1 & 1 & -1 & -1 \\ 1 & -1 & -1 & 1 \end{pmatrix} \begin{pmatrix} 1 \\ 0 \\ 0 \\ 0 \end{pmatrix} = \frac{1}{2} \begin{pmatrix} 1 \\ 1 \\ 1 \\ 1 \end{pmatrix}. \quad (2)$$

Suppose $x_0 = 3$. The operator for $I_{\tau=3}$ is

$$I_{\tau=3} = I_3 = C = \begin{pmatrix} 1 & 0 & 0 & 0 \\ 0 & 1 & 0 & 0 \\ 0 & 0 & 1 & 0 \\ 0 & 0 & 0 & -1 \end{pmatrix}, \quad (3)$$

which changes the phase of state $|00\rangle$ by π . Next we perform

$$\begin{aligned} D &= UQ = UI_{\gamma=0}U^{-1} = \\ &= \frac{1}{2} \begin{pmatrix} -1 & 1 & 1 & 1 \\ 1 & -1 & 1 & 1 \\ 1 & 1 & -1 & 1 \\ 1 & 1 & 1 & -1 \end{pmatrix} \end{aligned} \quad (4)$$

to obtain the final result:

$$|\psi_f\rangle = WQ|\psi_{in}\rangle = \begin{pmatrix} 0 \\ 0 \\ 0 \\ 1 \end{pmatrix}. \quad (5)$$

In the generalized quantum search algorithm, the phase inversions are replaced by arbitrary phase rotations. The corresponding operators, indicated by a “g” in the superscript, are

$$\begin{aligned} I_\gamma^g &= I - (1 - e^{i\theta})|\gamma\rangle\langle\gamma|, \\ I_\tau^g &= I - (1 - e^{i\phi})|\tau\rangle\langle\tau|, \\ Q^g &= -I_\gamma^g U^{-1} I_\tau^g U. \end{aligned} \quad (6)$$

When $\theta = \phi = \pi$ the original Grover algorithm is recovered. The operators in the example with 2 qubit for this generalized searching algorithm becomes, for $\tau = 3$,

$$C^g = I_{\tau=3}^g = I_3^g = \begin{pmatrix} 1 & 0 & 0 & 0 \\ 0 & 1 & 0 & 0 \\ 0 & 0 & 1 & 0 \\ 0 & 0 & 0 & e^{i\phi} \end{pmatrix}, \quad (7)$$

and

$$\begin{aligned} \mathcal{D}^g &= UQ^g = UI_{\gamma=0}^g U^{-1} \\ &= \begin{pmatrix} 1 & 1 & 1 & 1 \\ 1 & -1 & 1 & -1 \\ 1 & 1 & -1 & -1 \\ 1 & -1 & -1 & 1 \end{pmatrix} \begin{pmatrix} e^{i\theta} & 0 & 0 & 0 \\ 0 & 1 & 0 & 0 \\ 0 & 0 & 1 & 0 \\ 0 & 0 & 0 & 1 \end{pmatrix} \begin{pmatrix} 1 & 1 & 1 & 1 \\ 1 & -1 & 1 & -1 \\ 1 & 1 & -1 & -1 \\ 1 & -1 & -1 & 1 \end{pmatrix}. \end{aligned} \quad (8)$$

It has been proven that the generalized quantum searching algorithm can only find the marked state when the phase matching requirement $\theta = \phi$ is satisfied. When this requirement is not satisfied, the quantum algorithm will not work. In table 1, we give the state vector of the quantum computer in each step during a quantum searching process.

TABLES

TABLE I. Theoretical State Vector of the Register in Each Search Step

	phase matching $\theta = \phi = \pi/2$	phase mismatching $\theta = \pi/2, \phi = 3\pi/2$
step1:	$ \psi_1\rangle = 0.90 \tau\rangle + 0.43 c\rangle$	$ \psi_1\rangle = 0.25 \tau\rangle + 0.97 c\rangle$
step2:	$ \psi_2\rangle = 0.97 \tau\rangle + 0.22 c\rangle$	$ \psi_2\rangle = 0.62 \tau\rangle + 0.78 c\rangle$
step1:	$ \psi_3\rangle = 0.65 \tau\rangle + 0.76 c\rangle$	$ \psi_3\rangle = 0.063 \tau\rangle + 1.0 c\rangle$
step1:	$ \psi_4\rangle = 0.39 \tau\rangle + 0.92 c\rangle$	$ \psi_4\rangle = 0.59 \tau\rangle + 0.80 c\rangle$
step1:	$ \psi_5\rangle = 0.78 \tau\rangle + 0.62 c\rangle$	$ \psi_5\rangle = 0.36 \tau\rangle + 0.93 c\rangle$
step1:	$ \psi_6\rangle = 1.0 \tau\rangle + 0.014 c\rangle$	$ \psi_6\rangle = 0.41 \tau\rangle + 0.91 c\rangle$
step1:	$ \psi_7\rangle = 0.80 \tau\rangle + 0.60 c\rangle$	$ \psi_7\rangle = 0.57 \tau\rangle + 0.82 c\rangle$
step1:	$ \psi_8\rangle = 0.40 \tau\rangle + 0.92 c\rangle$	$ \psi_8\rangle = 0.13 \tau\rangle + 0.99 c\rangle$
step1:	$ \psi_9\rangle = 0.63 \tau\rangle + 0.77 c\rangle$	$ \psi_9\rangle = 0.63 \tau\rangle + 0.78 c\rangle$
step1:	$ \psi_{10}\rangle = 0.97 \tau\rangle + 0.24 c\rangle$	$ \psi_{10}\rangle = 0.19 \tau\rangle + 0.98 c\rangle$

III. THE PULSE SEQUENCE

In the experiment, the working media is H_2PO_3 . The molecular formula is given in Fig 1. The observed J-coupling between 1H and ^{31}P is 647.451 Hz. The experiment was performed on a Bruker 500 ARX NMR spectrometer. The frequencies for 1H and ^{31}P are about 500MHz 220MHz respectively. The Hamiltonian for this system can be modelled as a two-spin system with a Zeeman interaction,

$$H = \omega_A I_{AZ} + \omega_B I_{BZ} + 2\pi J_{AB} I_{AZ} I_{BZ}, \quad (9)$$

where $I_{AZ} = \frac{1}{2}\sigma_{ZA}$ is the angular momentum operator in the $\hat{\mathbf{e}}_z$ direction for spin A. ω_A and ω_B describe the strength of radio-frequency (rf) pulse which are applied on resonance to perform single-spin rotations to each of the two spins. The magnetic field is in $-\hat{\mathbf{e}}_z$ direction. From this hamiltonian, we construct three operators:

$$\begin{aligned} X^\theta &: \exp[-i\theta I_x/2] \text{rotation about } \hat{x}\text{axis through } \theta, \\ \overline{X^\theta} &: \exp[i\theta I_x/2] \text{rotation about } \hat{x} \text{ axis through } -\theta, \\ Y^\theta &: \exp[-i\theta I_y/2] \text{rotation about } \hat{y} \text{ axis through } \theta, \\ \overline{Y^\theta} &: \exp[i\theta I_y/2] \text{rotation about } \hat{y} \text{ axis through } -\theta, \end{aligned}$$

where subscript specifies the spin affected. $\tau^t = \exp[-2\pi i J_{AB} I_{ZA} I_{ZB}]$ is a soft-pulse which corresponds to a unitary transformation the system undergoes during period t in the doubly rotating frame. In the experiment, we denote $|\uparrow\rangle = |0\rangle$ and $|\downarrow\rangle = |1\rangle$. We used temporal averaging [8] to produce the effective pure state $|00\rangle$. The operation we used are

$$\begin{aligned} P_0 &: I(\text{none}) \\ P1 &: Y_B^{\frac{\pi}{2}} \tau^{\frac{1}{2J}} X_B^{\frac{\pi}{2}} Y_A^{\frac{\pi}{2}} \tau^{\frac{1}{2J}} X_A^{\frac{\pi}{2}} \\ P2 &: Y_A^{\frac{\pi}{2}} \tau^{\frac{1}{2J}} X_B^{\frac{\pi}{2}} X_A^{\frac{\pi}{2}} \tau^{\frac{1}{2J}} X_B^{\frac{\pi}{2}} \end{aligned} \quad (10)$$

The Walsh-Hadamard transform W was realized by

$$W = (X_A^{\frac{\pi}{2}})^2 \overline{Y_A}^{\frac{\pi}{2}} (X_B^{\frac{\pi}{2}})^2 \overline{Y_B}^{\frac{\pi}{2}}.$$

The operator C^g was realized by

$$C^g = Y_A^{\frac{\pi}{2}} \overline{X_A}^{\frac{\phi}{2}} \overline{Y_A}^{\frac{\pi}{2}} Y_B^{\frac{\pi}{2}} \overline{X_B}^{\frac{\phi}{2}} \overline{Y_B}^{\frac{\pi}{2}} \tau^{\frac{2\pi-\phi}{2J\pi}}.$$

And the operator $D^g = WQ^g = WI_0^gW$ was realized by:

$$D = Y_A^{\frac{\pi}{2}} X_A^{\frac{\theta}{2}} \overline{Y_A}^{\frac{\pi}{2}} Y_B^{\frac{\pi}{2}} X_B^{\frac{\theta}{2}} \overline{Y_B}^{\frac{\pi}{2}} \tau^{\frac{2\pi-\theta}{2J\pi}}.$$

One complete search iteration $O = DC$ can be simplified by combining sequential rotation and the result is

$$O = \overline{X_A}^{\frac{\theta}{2}} Y_A^{\frac{\pi}{2}} X_B^{\frac{\theta}{2}} Y_B^{\frac{\pi}{2}} \tau^{\frac{2\pi-\theta}{2J\pi}} X_A^{\frac{\phi}{2}} \overline{Y_A}^{\frac{\pi}{2}} X_B^{\frac{\phi}{2}} \overline{Y_B}^{\frac{\pi}{2}} \tau^{\frac{2\pi-\phi}{2J\pi}}.$$

IV. EXPERIMENTAL RESULTS AND DISCUSSIONS

In our experiment, two sets of experiments: one with $\theta = \phi = \frac{\pi}{2}$ in which phase matches and the other with $\theta = \frac{\pi}{2}, \phi = \frac{3\pi}{2}$ which is phase-mismatching. We used state tomography to obtain the density matrices [9]. The experimentally observed density matrices are given in Fig.2. In Fig.2, "reth1" means the real part of theoretical calculation for the 1st step.

TABLE II. The errors of the experiments

	$\theta = \phi = \frac{\pi}{2}$	$\theta = \frac{\pi}{2}, \phi = \frac{3\pi}{2}$
Step1	%27	%27
Step2	%35	%35
Step3	%30	%45
Step4	%34	%36
Step5	%41	%32
Step6	%35	%33
Step7	%20	%23
Step8	%69	%49
Step9	%30	%45
Step10	%37	%51

”rexp1” is the real part of experimental observed density matrix for the 1st step. Accordingly, ”imth1” means the theoretical result of the imaginary part of the density matrix for the 1st step, ”imexp1” is the corresponding results from experiment. The result with $\theta = \pi/2, \phi = 3\pi/2$ are given in Fig.3.

From these figures, it is seen that the agreement between theoretical predictions and experimental data is good. In particular, when phase matching is satisfied, the algorithm can find the marked state. However, when the phase matching requirement is not satisfied, the probability of finding the marked state is very low. We have plotted the probability for finding the marked state in each step in Fig4. It is apparent that phase matching is important.

There are several issues related to NMR quantum computing. First, there have been an on-going debate on the quantum nature of NMR quantum computing [10–12]. We have shown in [12] the quantum mechanical nature of NMR quantum computing. We will not go further to that issue. Secondly, the errors in NMR experiment is quite high. In table 2, we have given the relative error defined as $\delta\rho = \frac{\|\rho_{th} - \rho_{exp}\|}{\|\rho\|}$. There are several reasons for this large errors. The main cause of error is errors occurred while doing the integration of areas of the spectrum. In particular, the quality of signals from ^{31}P is poor. It is estimated that errors arising area integration can be upto 50% for typical NMR technique, especially when the area is small. This “artificial” error has washed out the genuine error during the quantum computation. The other source of error [13,14] are gate imperfections and decoherence which are genuine errors in a quantum computation. It is anticipated that the decoherence effects due to the uncontrolled interaction of the system with surrounding environment is weak at the early stages of a quantum computation. Errors arising from imperfect gate operations occur at constant rate. As both decoherence and imperfect gate operations contribute to the total error, the accumulating effect will leads to increased errors at later stages. This anticipation is not true here. The relative errors at later stages are sometimes even smaller than the early stages. For instance at step 7 in the phase-matching case, the relative error is only 20%, the smallet among the 10 steps. This can be easily understood because the “artificial” errors introduced in the area integration is very much. The relative error reflects mainly the errors caused by them. Similar result is observed in other NMR quantum computing experiment, for instance in [5]. To get a conclusion about the “genuine” error during quantum computing, one has to use an NMR spectrometer tailored for quantum computing and improve the accuracy in constructing the density matrix. Though the relative errors are large, the density matrices are sufficient for us to demonstrate the effect of phase matching in quantum searching.

Thirdly, the construction of the density matrix is very time-consuming. It is managable while the number of qubit is small. When the qubit number becomes large, it is prohibitively difficult to construct them. However, this is not detrimental to quantum computing, since in quantum computing we need only a simultaneous measurement on each of the qubit to see whether it is up or down. However, when the number of qubit is small and a construction of the density matrix is possible, such information is very helpful. It can be served as a benchmark test, especially on the accuracy of the quantum computation.

In summary, phase matching in quantum searching is explicitly demonstrated in a 2 qubits NMR system. The experimental results are in agreement with theoretical predictions.

This work is support in part by China National Science Foundation, the excellent uni-

versity teacher's fund of China Education Ministry, Fok Ying-Tung education foundation.

REFERENCES

- [1] L.K. Grover, Phys. Rev. Lett 79(1997)325
- [2] L.K. Grover, Phys. Rev. Lett 80(1998)4329
- [3] G.L. Long et al, Commun. Theor. Phys 32(1999)335
- [4] G.I. Long et al, Phys. Lett. A 262(1999)27
- [5] I.L. Chuang et al, Phys. Rev. Lett 80(1998)3408
- [6] J.A. Jones et al, Nature, 393(1998)344
- [7] L.M.K. Vandersypen et al, Appl. Phys. Lett. 76(2000)646
- [8] E. Knill, I.L. Chuang et al, Phys. Rev A 57(1998) 3348
- [9] I.L. Chuang et al, Proc. R. Soc. Lond A 454Z(1998) 447
- [10] S. L. Braunstein et al, Phys. Rev. Lett. 83(1999) 1054
- [11] R. Laflamme, <http://quickreviews.org/>
- [12] G. L. Long et al, quant-ph/007077
- [13] G.L. Long et al, Phys. Rev A 61(2000)042305
- [14] B. Pablo-Norman and M. Ruiz-Altaba, Phys. Rev. A61(2000)012301

Figure captions

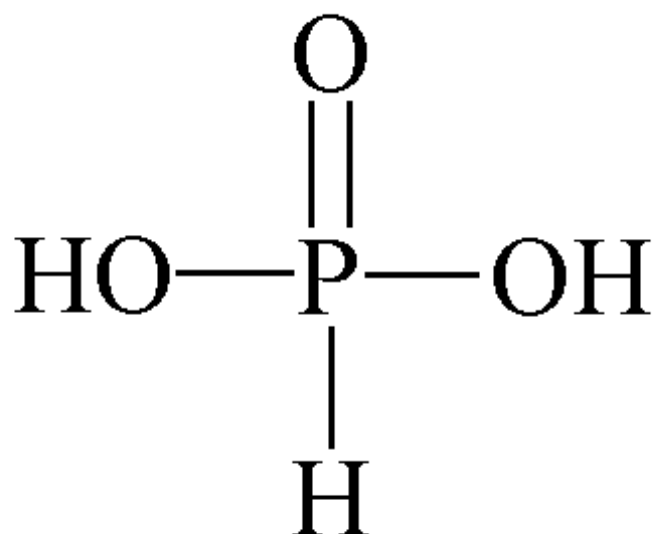
Fig.1 The structural formula of H_2PO_3

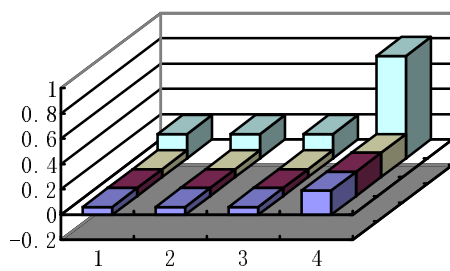
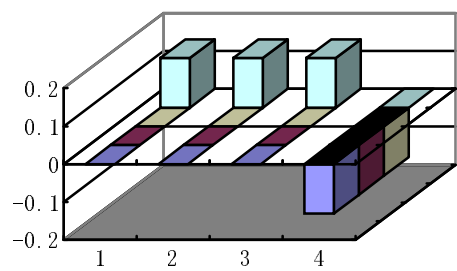
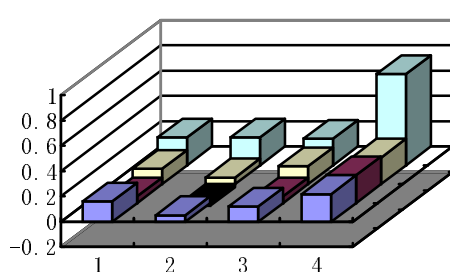
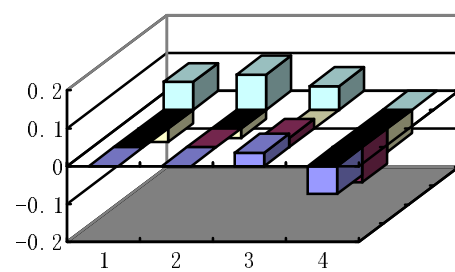
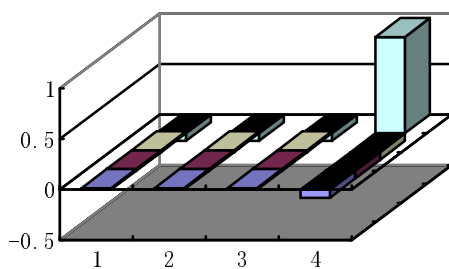
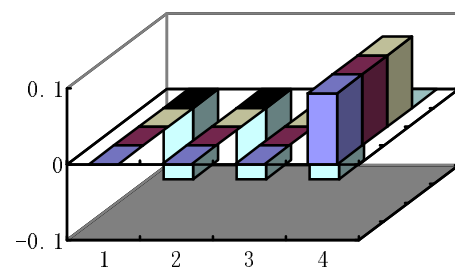
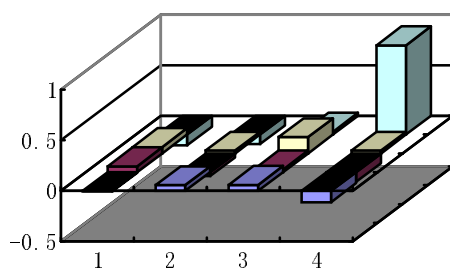
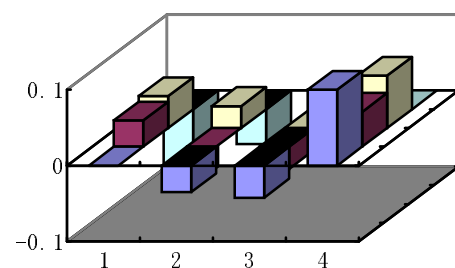
Fig.2 Comparisons of theoretical and experimental density matrices with $\theta = \phi = \pi/2$:(a) for steps 1 and 2; (b) for steps 3 and 4;(c) for steps 5 and 6; (d) for steps 7 and 8; (e) for steps 9 and 10. The meaning of the symbols above each diagram is: "re" =real part, "im"=imaginary part, "th"=theoretical, "exp"=experimental. The last one, a number is the searching step number. Fig.3 Same as Fig.2 but for $\theta = \pi/2, \phi = 3\pi/2$.

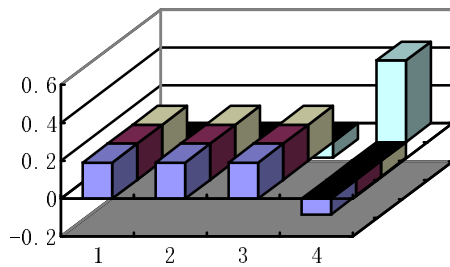
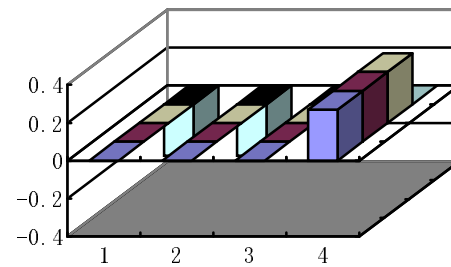
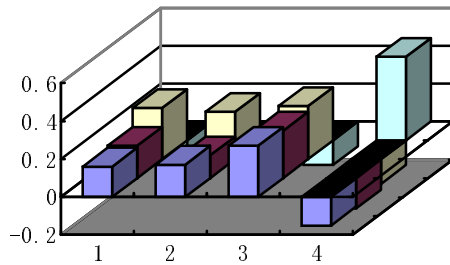
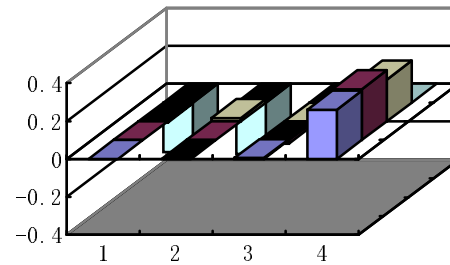
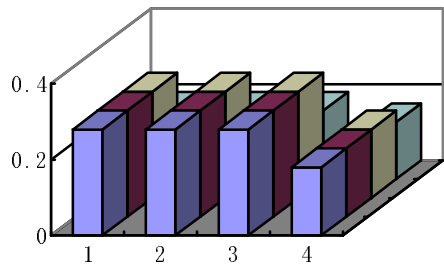
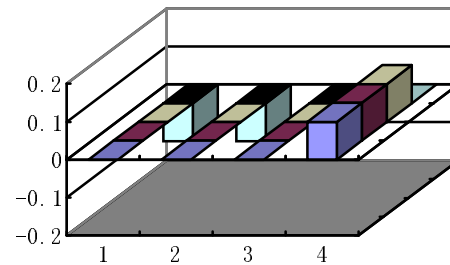
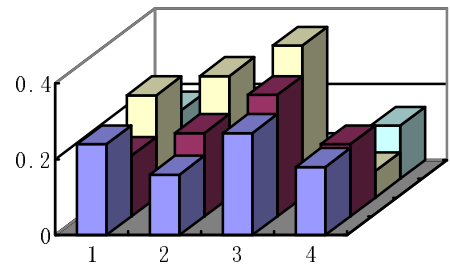
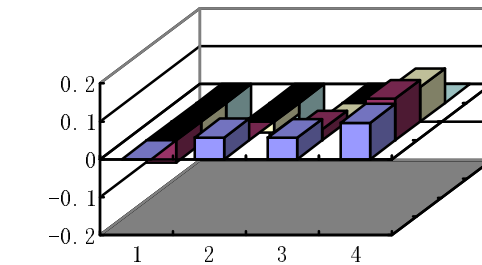
Fig.4 Comparisons of theoretical and experimental percentage probability of finding a marked state of $\theta = \phi = \pi/2$.

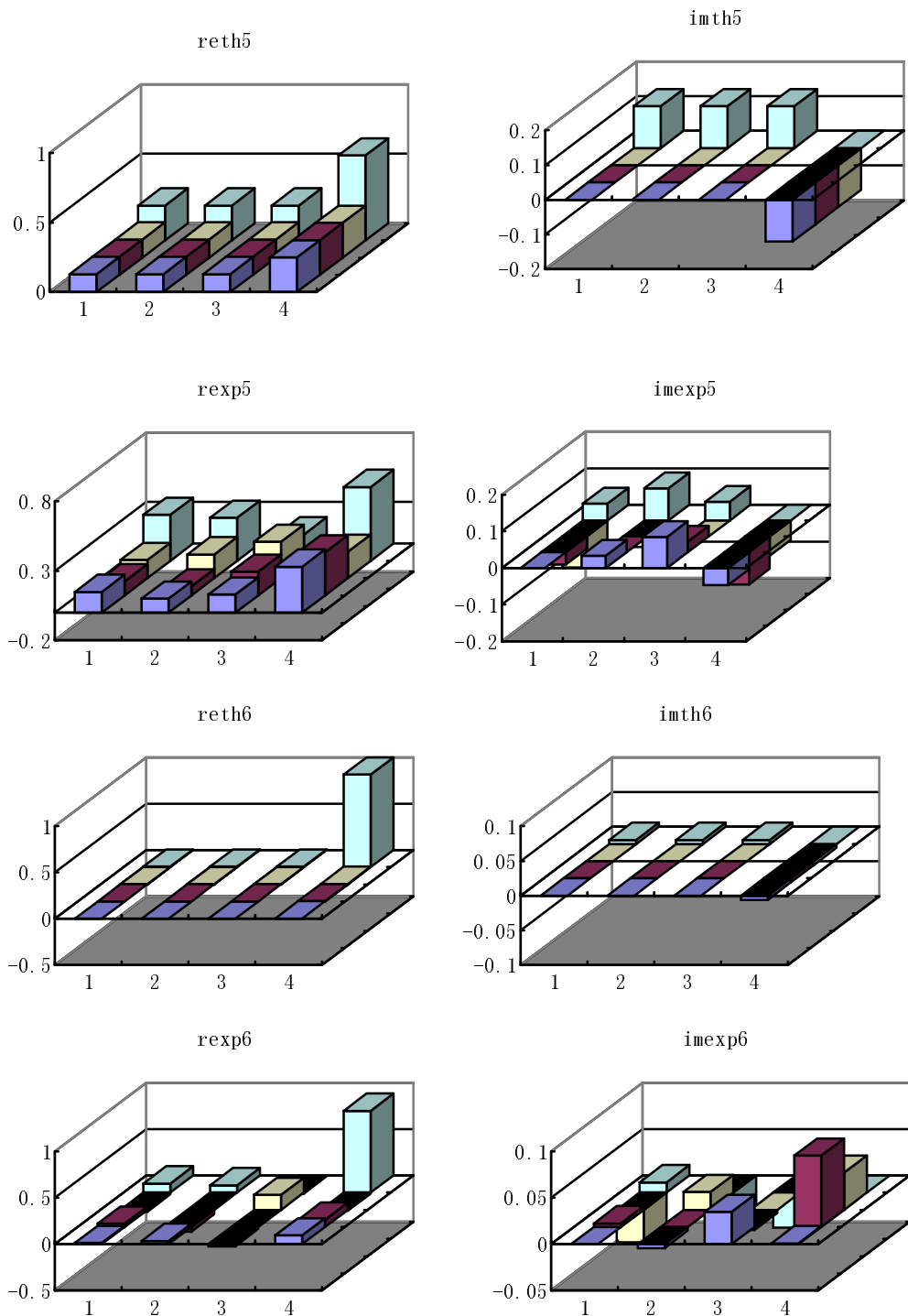
Fig.5 Comparisons of theoretical and experimental percentage probability of finding a marked state of $\theta = \pi/2, \phi = 3\pi/2$.

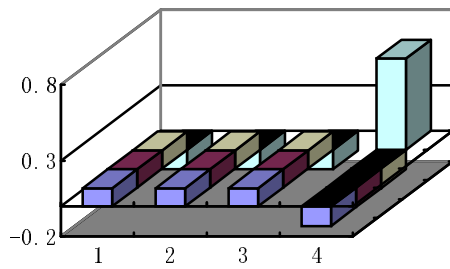
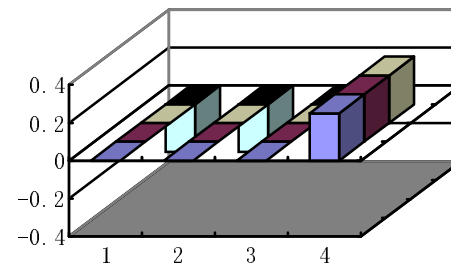
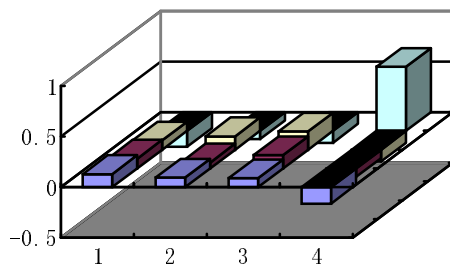
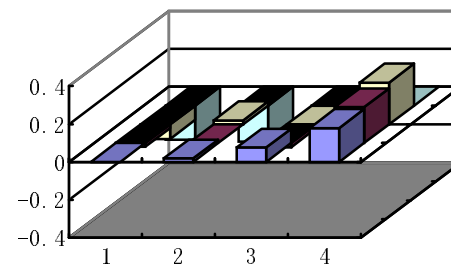
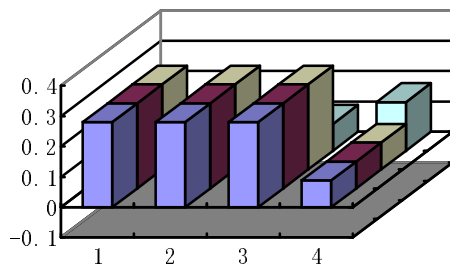
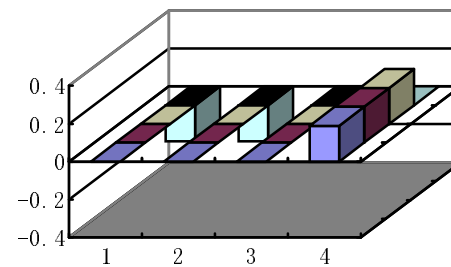
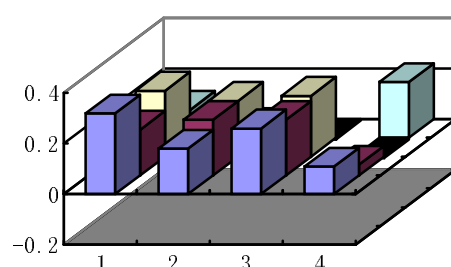
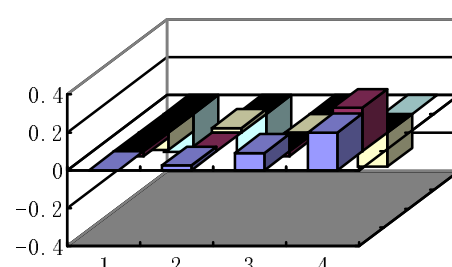
h2po3.bmp (561x381x16M bmp)

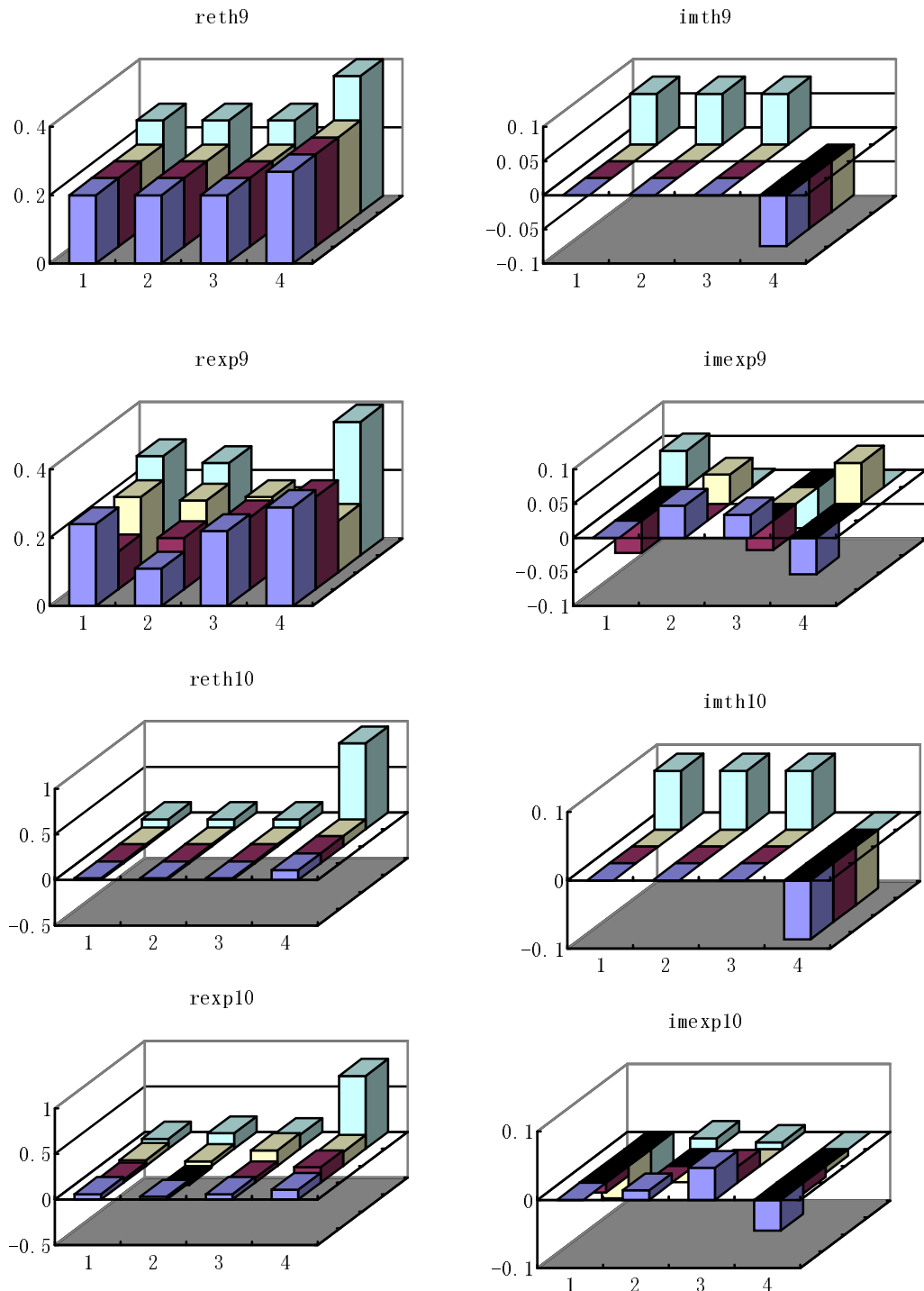


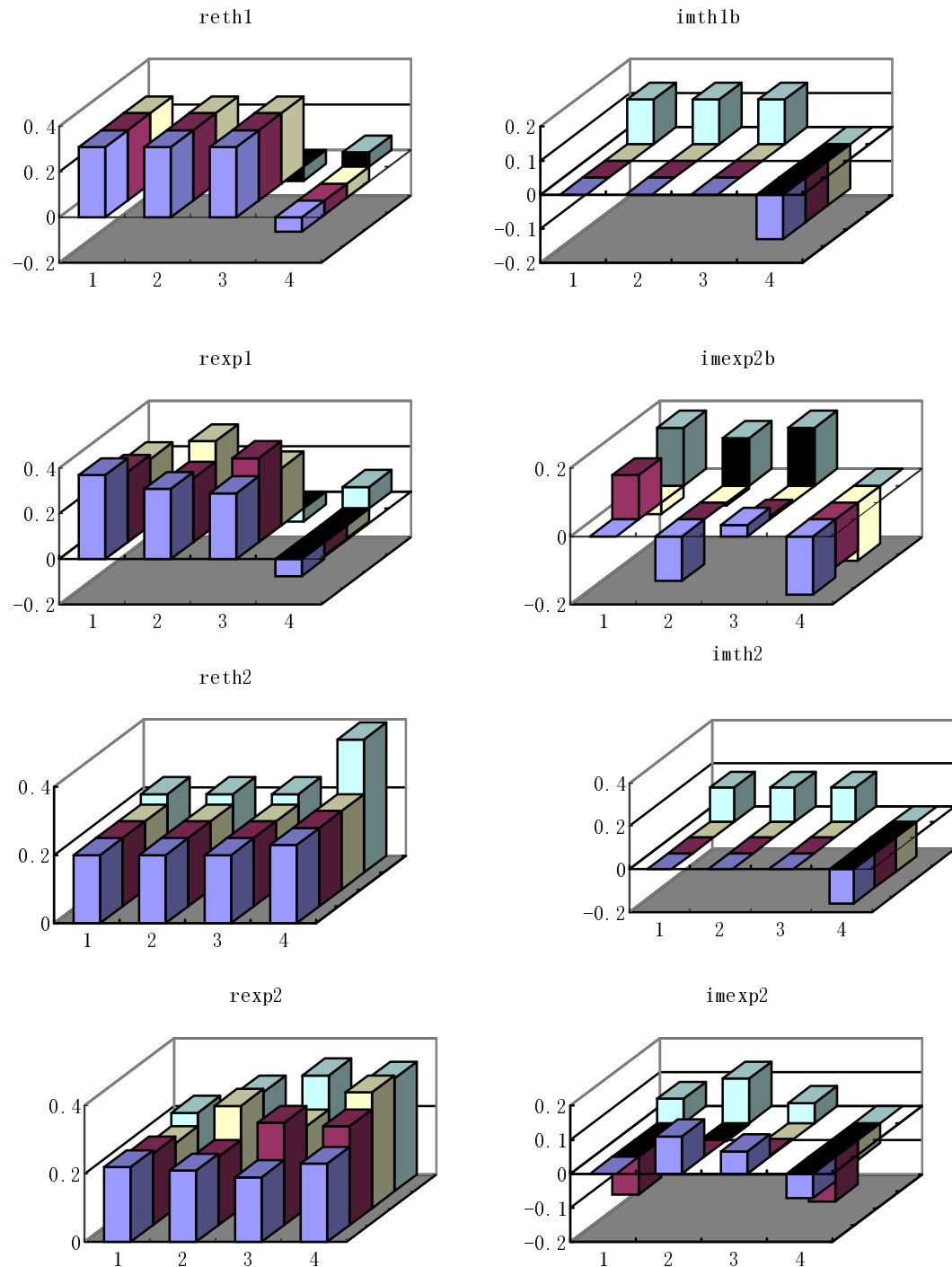
r_{eth1}i_{th1}r_{exp1}i_{exp1}r_{eth2}i_{th2}r_{exp2}i_{exp2}

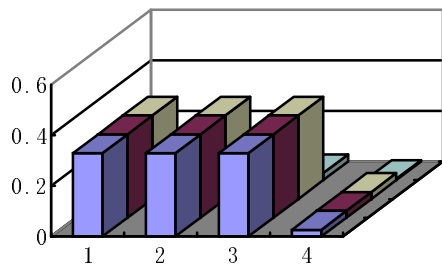
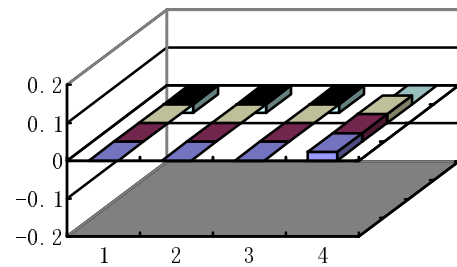
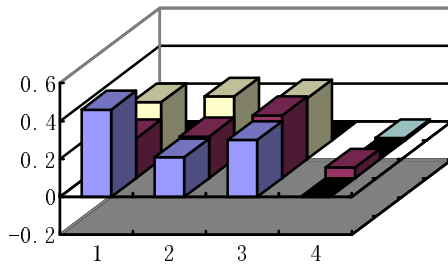
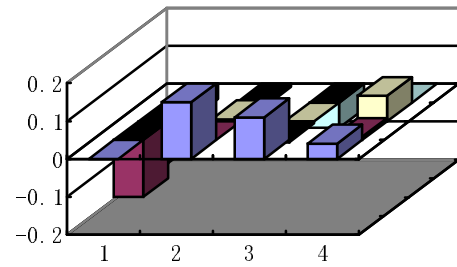
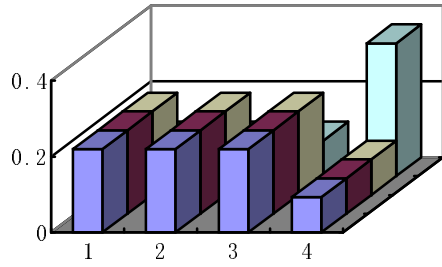
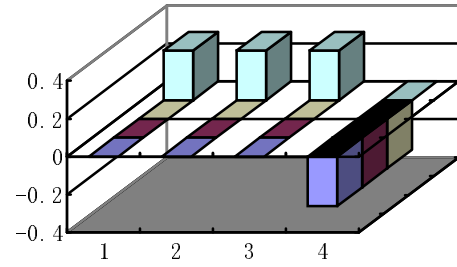
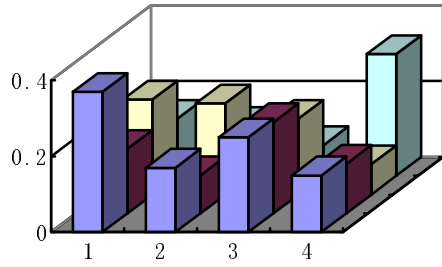
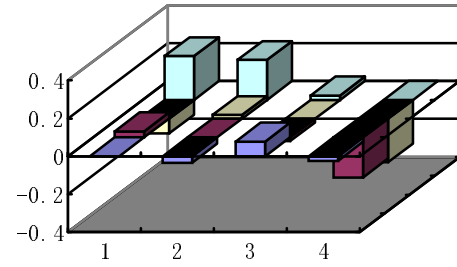
r_{eth3}i_{mth3}r_{exp3}i_{mexp3}r_{eth4}i_{mth4}r_{exp4}i_{mexp4}

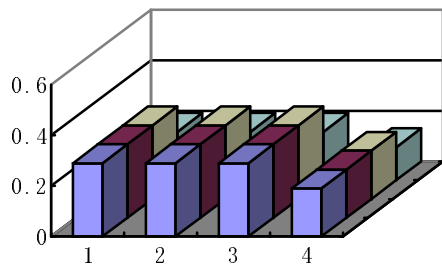
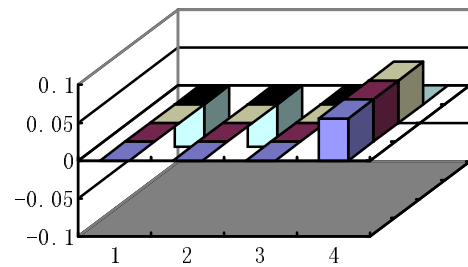
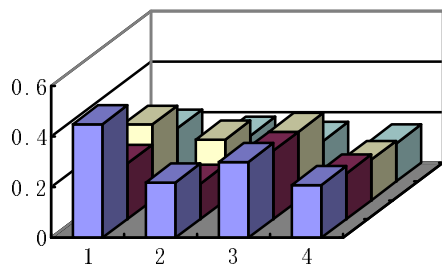
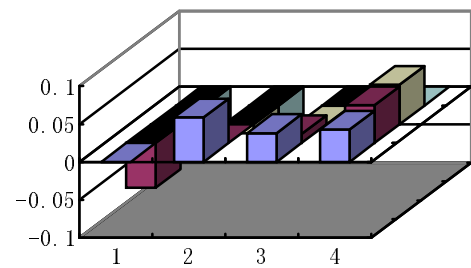
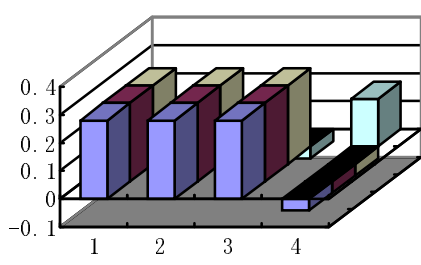
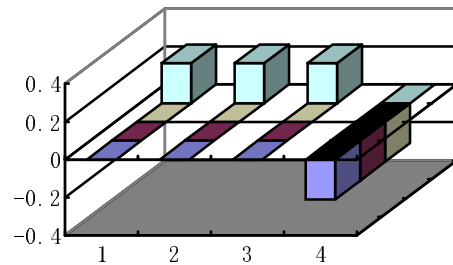
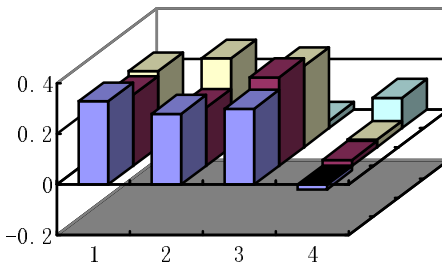


r_{eth}7i_{th}7r_{exp}7i_{exp}7r_{eth}8i_{th}8r_{exp}8i_{exp}8





r_{eth3}i_{mth3b}r_{exp3}i_{mexp3}r_{eth4}i_{mth4}r_{exp4}i_{mexp4}

r_{eth}5i_{th}5r_{exp}5i_{exp}5r_{eth}6i_{th}6r_{exp}6i_{exp}6